
PERGAMON

Journal of the Mechanics and Physics of Solids
48 (2000) 797–826

JOURNAL OF THE
MECHANICS AND
PHYSICS OF SOLIDS

www.elsevier.com/locate/jmps

Numerical experiments in revisited brittle fracture

B. Bourdin, G.A. Francfort, J-J. Marigo*

Institut Galilée, Université Paris-Nord, 93430, Villetaneuse, France

Received 4 November 1998; received in revised form 26 March 1999

Abstract

The numerical implementation of the model of brittle fracture developed in Francfort and Marigo (1998. J. Mech. Phys. Solids 46 (8), 1319–1342) is presented. Various computational methods based on variational approximations of the original functional are proposed. They are tested on several antiplanar and planar examples that are beyond the reach of the classical computational tools of fracture mechanics. © 2000 Elsevier Science Ltd. All rights reserved.

Keywords: A. Fracture; Fracture toughness; C. Energy methods; Variational calculus; Finite elements

1. Introduction

The present work follows in the footsteps of a previous study (Francfort and Marigo, 1998) where a variational model for quasistatic crack evolution in a brittle material is proposed. Its merits and drawbacks are elaborated upon in Francfort and Marigo (1998) and we will presently refrain from any further comments, so as to concentrate instead on a numerical feasibility study. Our goal is to convince the reader that the model lives up to its theoretical expectation and is a useful and manageable predictive tool. To this end, we will confront settings that are beyond the scope of the usual computational arsenal of the investigator

* Corresponding author.
E-mail address: marigo@lpmtm.univ-paris13.fr (J.J. Marigo).

PII: S0022-5096(99)00028-9

in the field; we will demonstrate that a carefully tailored numerical version of the model does not stall in such hostile environments but delivers crack evolutions which fit squarely within the proposed framework.

Of course, we still fall short of the ultimate goal of any predictive theory, namely the corroboration and prediction of experimental results. Such a goal cannot be contemplated without prior internal review of the self-consistency of the model. This is how the present work should be viewed, although we do not turn a blind eye to experimental results, whenever they are known to us. But, in all fairness, such comparisons can only be qualitative in the absence of a detailed experimental/numerical protocol. We do hope to be able, in the not too distant future, to report on the success—or failure—of such an undertaking.

Let us now briefly recapitulate the main features of the model in an exemplary setting: a homogeneous two-dimensional elastic body Ω with elasticity tensor A and fracture toughness k is submitted to an imposed displacement field $U(t, x)$ on the part $\partial\Omega\backslash\mathcal{N}$ of its boundary and free of tractions on the complementary part $\mathcal{N}$ of that boundary. We further assume that, at time $t = 0$, the body Ω is uncracked and that $U(t, x) = tU(x)$, where $U(x)$ is a smooth displacement field. If Γ is a crack, a compact in $\bar{\Omega}$ (the crack may go to the boundary), its surface energy is

$$E_s(\Gamma) = k\mathcal{H}^1(\Gamma\backslash\mathcal{N}),$$

where, here and in the remainder of the paper, $\mathcal{H}^{n-1}$ denotes the $n-1$-dimensional Hausdorff measure, a measure which coincides with the usual surface measure for smooth enough hypersurfaces of $\mathbf{R}^n$. Note that the surface energy will be infinite for cracks that are too fat, i.e., with infinite one-dimensional Hausdorff measure. Note also that this definition of the surface energy slightly departs from that proposed in Francfort and Marigo (1998); the resulting formulation will, however, be equivalent.

We now define the bulk energy as

$$E_e(\Gamma, t) = \inf_w \left\{ \int_{\Omega\backslash\Gamma} Ae(w) \cdot e(w) \mathrm{d}x; w = U(t) \quad \text{on } \partial\Omega\backslash(\mathcal{N} \cup \Gamma) \right\},$$

where $e(w) = 1/2(\nabla w + \nabla w^t)$. A more precise definition is given in Francfort and Marigo (1998). It is worth emphasizing that the bulk energy is not a minimum, but merely an infimum because the infimum might not be attained if Γ is not smooth 'enough'.

The total energy is defined as

$$E(\Gamma, t) = E_s(\Gamma) + E_e(\Gamma, t).$$

The evolution of the crack is then governed by the following law (see Law 2.9 in Francfort and Marigo, 1998):

1. $\Gamma(t)\nearrow$ with t with $\Gamma(t) = \emptyset$, $t < 0$,

2. $E(\Gamma(t), t) \leq E(\Gamma, t)$, for any $\Gamma \supset \cup_{s<t}\Gamma(s)$,
3. $E(\Gamma(t), t) \leq E(\Gamma(s), t)$, for all $s < t$.

As noted in Francfort and Marigo (1998) the first condition forces the crack to grow with time, the second states that the total energy of the actual crack is minimal among all cracks that are compatible with the fracture state at the current time, while the third and surprising condition forces the crack to keep track of its prior energetic states. The latter condition is shown in Francfort and Marigo (1998) to amount to a selection criterion among possible crack evolutions (see Remark 4.18 in Francfort and Marigo, 1998). Remark also that fat cracks are prohibited by condition (2).

The search for global minimizers might be too difficult a task for an actual material whenever energy barriers surround a 'metastable state'. In such a situation, it is certainly more realistic for the material to remain in that metastable state. In mathematical terms, local minimizers should provide a more accurate description of crack evolution. This is not taken into consideration in the proposed model, although it is the object of ongoing research. In any case, global minimization delivers the worst case scenario for quasistatic crack growth. Further, note that the lack of convexity of the relevant energies may lead the numerical schemes to actually detect local rather than global minimizers.

Whenever time is discretized—which is certainly the case in any numerical simulation—and the time steps are $t_0 = 0 \leq t_1 \leq \cdots \leq t_p \leq \cdots$, conditions (1)–(3) degenerate into

1. $\Gamma_i \supset \Gamma_{i-1}$,
2. $E(\Gamma_i, t_i) \leq E(\Gamma, t_i)$, for all $\Gamma \supset \Gamma_{i-1}$,

which is more readily interpreted than its continuous analogue.

Our goal is to implement the discretized scheme in a realistic setting. A brute force approach is doomed because we do not a priori know the locus of the optimal crack at time t_i. The two methods detailed in Section 2 address the aforementioned issue. Both are based on the concept of Γ-convergence which describes in mathematical terms how a sequence of functionals depending on a parameter converges to the desired functional as that parameter tends to 0 (see Section 2).

The first method introduces a two-field functional; the first field approximates the solution-displacement field for the given boundary displacement and fore the solution-crack while the second is a field that varies between 0 and 1, takes the value 0 near the crack and 1 away from it. This functional, which has been introduced in the context of image segmentation in Ambrosio and Tortorelli (1990), is a continuous two-field functional. It has to be further discretized, so as to become amenable to numerical implementation. The functional, its discretization and associated issues are discussed in Subsection 2.1.

The second method goes directly to the discrete level by introducing a one-field

functional defined on a triangulation of the domain. In essence, it is also a two-field functional, but the second field is a triangulation. That functional and associated issues are discussed in Subsection 2.2.

The short Subsection 2.3 aims at comparing the two methods and refers for such a task to the example developed in Subsection 3.1.

Subsection 2.4 mentions the additional theoretical hurdles raised by a plane elasticity setting.

Section 3 is devoted to the computation of three evolutions that illustrate the flexibility of the methods introduced in Section 2. Subsection 3.1 investigates the tearing of a rigid reinforcement in an elastic matrix; Subsection 3.2 looks at crack growth in a fiber reinforced rectangular matrix submitted to monotonically increasing displacements on one of its sides; Subsection 3.3 follows the mixed mode propagation of a pre-existing crack in a rectangular plate.

Unfortunately, the intricacies of the proposed schemes are, as in all numerical studies, of a mathematical nature. Although we made every feasible attempt to keep technicalities to the bare minimum, we could not ignore or bypass notions such as Γ-convergence, because those are at the root of a satisfactory handling of the model. The mechanical soundness of the model cannot be found in its numerical implementation, but rather in the results that such an implementation will produce. Therefore, a reader merely interested in confronting the model with his or her own mechanical intuition is urged to skip Section 2 and to ponder the examples presented in Section 3; such a reader, as well as others, should however, refrain from lending mechanical significance to the approximations discussed in Section 2.

2. Numerical implementation of the model

This section is devoted to an exposition of two numerical methods that are suited to the implementation of the model presented in the introduction.

Our model of brittle fracture is close to a model of image segmentation, namely that obtained through the minimization of the Mumford–Shah functional (Mumford and Shah, 1989); the latter has been thoroughly investigated in recent years. For a given grey level image (i.e., a real valued function g, defined on a bounded open domain Ω), the goal is to minimize the following energy

$$\int_{\Omega\setminus K} |\nabla u|^2 + |u-g|^2 \, \mathrm{d}x + \mathscr{H}^{n-1}(K),$$

over each compact subset of $\mathbf{R}^n$, K (the 'edge set' of the image) and each real valued function u (the 'segmented image'), continuous on $\Omega\setminus K$.

From a mathematical standpoint this minimization problem is awkward, mainly because it is not easy to see how to topologize such compact sets. The remarkable 'trick' used in De-Giorgi et al. (1989) is to resort to an adequate weak formulation of this problem in a framework that is more classical from the standpoint of the

calculus of variations, albeit at the expense of using a somewhat exotic functional space, the space of special bounded variation functions, SBV(Ω), a space introduced in Ambrosio (1990) which allows for jump discontinuities in the fields (the jump set of an element u in SBV(Ω) is denoted by S_u). The weak functional is then defined as

$$\int_\Omega \mid \nabla v \mid^2 + \mid v - g \mid^2 \ \mathrm{d}x + \mathscr{H}^{n-1}(S_v \cap \Omega).$$

Using results in Ambrosio (1989a, 1989b, 1990), the latter is shown in De-Giorgi et al. (1989) to admit a minimum u in SBV(Ω), and it is also shown there that the pair $(u, \overline{S_u})$ is a solution to the original problem.

The weak formulation provides a good starting point for a numerical implementation of the Mumford–Shah model. That this is so is not obvious at first glance because functions of SBV(Ω) can exhibit jump discontinuities on arbitrary 'smooth' lower-dimensional manifolds. A classical finite element method—or finite difference method, or any other method for that matter—is immediately doomed since the locus of the jump set is a priori unknown. The proposed methods rely on some kind of 'regularization' through Γ-convergence (see Ambrosio and Tortorelli, 1990, 1992; Chambolle and Dal Maso, 1998 for different regularizations). There is still the additional task of implementing a numerical method for the minimization of the regularized problem (Finzi-Vita and Perugia, 1995; Bourdin, 1999; Chambolle, 1999; Bourdin and Chambolle, in preparation; Bellettini and Coscia, 1994).

The antiplane isotropic elasticity case with constant elasticity and fracture toughness is the closest in spirit to the Mumford–Shah functional. In the former however, non-homogeneous Dirichlet boundary conditions will replace the $\int_\Omega |u-g|^2 \ \mathrm{d}x$ term while the set of admissible cracks will be somewhat different from the set of edges. Indeed, while in the image context, edges are to be detected inside the domain, cracks are to be accounted for inside and at the boundary of the domain. As such, the weak formulation cannot be a direct transposition of that established for the image problem. A similar difficulty has been addressed in Carriero and Leaci (1990) through the use of an extension of the boundary condition to the whole space $\mathbf{R}^n$. This method will be slightly modified so as to be in a position to treat a mixed boundary value problem.

The numerical models used for the isotropic antiplane case with constant toughness are described below. Their extension to plane elasticity is also discussed. The mathematical details are kept to the absolute minimum and the interested reader should refer to the quoted references for a rigorous study. Firstly, we present the weak formulation and explain how boundary conditions are dealt with, then we suggest two regularizations of the resulting functional and detail their implementations. Finally, a comparison between those is conducted on a test case (see Subsection 3.1).

In what follows, Ω denotes a bounded open domain of $\mathbf{R}^2$ with piecewise Lipschitz boundary and U, a $W^{1,\infty}$ function. The variational model for brittle

fracture described in this section is applied to an isotropic antiplane case with constant fracture toughness and, for the sake of simplicity, we will assume that the toughness is 1 and that the Lamé coefficient μ is 2. Note however, that general values of μ can be recovered by a change of scales, because the energy is not scale invariant. The 'strong' problem is given by the functional

$$\mathscr{E}(u, K) = \int_{\Omega\backslash K} |\nabla u|^2 \, \mathrm{d}x + \mathscr{H}^1(K \cap \bar{\Omega}),$$

for each admissible crack set $K \subset \bar{\Omega}$ and each admissible function, $u \in W^{1,2}(\Omega\backslash K)$ such that $u = U$ on a part of $\partial\Omega$, denoted by $\mathscr{D}$, and such that $\partial u/\partial n = 0$ on $\mathscr{N} = \partial\Omega\backslash\mathscr{D}$. As noted above, the formulation must allow for jumps of u on $\partial\Omega$. Thus, the function $\mathscr{E}$ is redefined on a 'large enough' open set $\tilde{\Omega}$, containing $\bar{\Omega}$ (an estimate of 'how large' $\tilde{\Omega}$ should be will be given). We are now in a position to lend a meaning to the Dirichlet boundary condition U upon replacing the set of admissible functions by the set of $W^{1,2}(\tilde{\Omega}\backslash K)$-functions with prescribed value U on $\tilde{\Omega}\backslash\bar{\Omega}$. We have, however, lost the traction-free boundary conditions on $\mathscr{N}$. They are recovered by allowing $\tilde{\Omega}$ to experience free cracking wherever the normal derivative of the function u should be zero. The surface energy is thus computed on $\bar{\Omega}\backslash\mathscr{N}$ [i.e., $\mathscr{H}^1(K)$ is replaced by $\mathscr{H}^1(K\backslash\mathscr{N})$]. The mixed boundary problem is

$$(\mathscr{P}): \begin{cases} \text{Find a compact subset } K \text{ of } \bar{\Omega}, \text{ and} \\ u \in \mathscr{U}_s = \{v \in W^{1,2}(\tilde{\Omega}\backslash(K \cup \mathscr{N})) \quad \text{such that } v = U \quad \text{on } \tilde{\Omega}\backslash\bar{\Omega}\}, \\ \text{that minimizes} \\ \mathscr{E}(v, K) = \displaystyle\int_{\Omega\backslash(K\cup\mathscr{N})} |\nabla v|^2 \, \mathrm{d}x + \mathscr{H}^1(S_v\backslash\mathscr{N}). \end{cases}$$

Note that such a procedure permits us to consider cracked domains with traction-free crack lips upon letting $\mathscr{N}$ be a subset of Ω instead of $\partial\Omega$.

It can be proved (see Bourdin, 1998) that the 'strong' problem is equivalent to the following 'weak' problem:

$$(P): \begin{cases} \text{Find } u \in \mathrm{SBV}(\tilde{\Omega}), \text{ such that } u = U \quad \text{on } \tilde{\Omega}\backslash\bar{\Omega}, \text{ minimizing} \\ \qquad E(v) = \displaystyle\int_{\Omega} |\nabla v|^2 \, \mathrm{d}x + \mathscr{H}^1(S_v\backslash\mathscr{N}) \\ \text{on } \mathscr{U}_w = \{v \in \mathrm{SBV}(\tilde{\Omega}) \quad \text{such that } v = U \quad \text{on } \tilde{\Omega}\backslash\bar{\Omega}\}. \end{cases}$$

In other words the problem $(\mathscr{P})$ admits $(u, \overline{S_u\backslash\mathscr{N}})$ as a minimum. Let us merely recall the main steps in the proof. It is firstly shown that if (u, K) is a minimizer for $(\mathscr{P})$, then u is an admissible function for (P) and its weak energy $E(u)$ is lower than or equal to its strong energy $\mathscr{E}(u, K)$. Then one establishes the existence of at least one solution to the weak problem and one shows that the associated jump set satisfies $\mathscr{H}^1((\overline{S_u\backslash\mathscr{N}})\backslash(S_u\backslash\mathscr{N})) = 0$ [i.e., $\mathscr{E}(u, \overline{S_u\backslash\mathscr{N}}) = E(u)$] which yields the existence of a solution to $(\mathscr{P})$.

The weak problem is closer to a standard minimization problem but does not

yet fit into an adequate framework for numerical implementation (the set K has been somehow 'artificially' removed in E, but the jump set S_u is still a problem as far as the numerical implementation is concerned). But, as will be seen below, a correct approximation of the weak problem is in turn amenable to numerical implementation.

The two methods introduced below make use of the same analytical tools. Formally, we build a sequence of regularized functional $\{E_c\}_c$ and successively prove its Γ-convergence to E, the existence of minimizers for each of its terms E_c and the compactness of the resulting sequence. We merely recall the definition of Γ-convergence and explain how the above quoted properties can give rise to an adequate numerical scheme. Let us define a functional G and a sequence $\{G_c\}_c$ on a functional space X. Then, $G_c\Gamma$ (τ)-converges to G when $c \to 0$ if the following properties are met by each function $u \in X$:

1. Each sequence of functions $\{u_c\}_c$ in X converging to u for the topology τ satisfies

$$\liminf_{c\to 0} G_c(u_c) \geq G(u).$$

2. There exists a sequence of functions $(u_c)_c$ in X that converges to u for the topology τ, such that

$$\limsup_{c\to 0} G_c(u_c) \leq G(u).$$

If both properties hold true, let $\{\tilde{u}_c\}_c$ be a sequence of minimizer for $\{G_c\}_c$. By the compactness property, there exists $\tilde{u} \in X$ such that, for a subsequence of $\tilde{u}_c$, still indexed by c, $\tilde{u}_c \xrightarrow{\tau} \tilde{u}$; by the estimate for the lower Γ-limit, one deduces that $\liminf_{c\to 0} G_c(\tilde{u}_c) \geq G(\tilde{u})$ and then by applying the estimate for the upper Γ-limit to the minimum for G, there exists, for each $v \in X$, a sequence $\{v_c\}_c$ converging to v such that

$$G(v) \geq \limsup_{c\to 0} G_c(v_c) \geq \liminf_{c\to 0} G_c(\tilde{u}_c) \geq G(\tilde{u}),$$

so that $\tilde{u}$ is a minimizer for G and $G_c(\tilde{u}_c) \xrightarrow{c\to 0} G(\tilde{u})$.

We are now in a position to introduce two different regularizations of the weak energy E in the antiplane case. While the first one is a straightforward adaptation of a well-known regularization of the Mumford–Shah problem (see Ambrosio and Tortorelli, 1990, 1992)—itself in the spirit of a result on the regularization of a phase transition problem (see Modica and Mortola, 1977)—the approach in the second one is totally different and extensively uses the mesh adaptation techniques. We will detail the computation of the first time step, according to the discrete time scheme introduced in Francfort and Marigo (1998) and extend both methods to the following time steps.

2.1. Approximation by an elliptic functional

In this subsection, we adapt the regularized formulation used in Ambrosio and Tortorelli (1992) to our problem and discuss its implementation.

The main idea in this kind of approximation is to introduce an auxiliary variable (subsequently denoted by v) that represents in some sense the jump set in E. In order to lend a meaning to the Γ-convergence of a two-field functional to a one-field one, it is convenient to extend the definition of E by setting

$$F(u, v) = \begin{cases} E(u) & \text{if } u \in \mathrm{SBV}(\tilde{\Omega}),\ u = U \text{ on } \tilde{\Omega}\backslash\bar{\Omega}, \text{ and } v = 1 \text{ a.e. on } \tilde{\Omega}, \\ +\infty & \text{otherwise,} \end{cases} \tag{1}$$

and to introduce the following regularized functional, for each $u \in W^{1,2}(\tilde{\Omega}\backslash\mathcal{N})$ and $v \in W^{1,2}(\tilde{\Omega}\backslash\mathcal{N}; [0, 1])$,

$$E_c(u, v) = \int_{\Omega\backslash\mathcal{N}} (v^2 + k_c) \mid \nabla u \mid^2 \, \mathrm{d}x + \int_{\tilde{\Omega}\backslash\mathcal{N}} \left(c \mid \nabla v \mid^2 + \frac{(1-v)^2}{4c} \right) \mathrm{d}x, \tag{2}$$

where k_c is a positive constant depending only on c. We then define

$$F_c(u, v) = \begin{cases} E_c(u, v) & \text{if } u \in W^{1,2}(\tilde{\Omega}\backslash\mathcal{N}),\ u = U \text{ on } \tilde{\Omega}\backslash\bar{\Omega}, \text{ and } v \in W^{1,2}(\tilde{\Omega}\backslash\mathcal{N};[0, 1]) \\ +\infty & \text{otherwise.} \end{cases} \tag{3}$$

Then, if $k_c \ll c$ when $c \to 0$, the following properties are proved:

1. F_c $\Gamma(L^2)$-converges to F as $c \to 0$.
2. There exists at least one minimizer (u_c, v_c) for E_c with prescribed value U on $\tilde{\Omega}\backslash\bar{\Omega}$.
3. The sequence of minimizers for F_c is compact in L^2.

Thus, in the limit the minimization of F and that of F_c are equivalent. The proofs of the Γ-limit estimates further demonstrate that the first part of the regularized energy $\int_{\Omega\backslash\mathcal{N}}(v^2 + k_c)|\nabla u|^2 \, \mathrm{d}x$ converges to the bulk energy $\int_{\Omega\backslash\mathcal{N}}|\nabla u|^2 \, \mathrm{d}x$ while the second one converges to the surface energy $\mathcal{H}^1(S_u\backslash\mathcal{N})$. Finally, the auxiliary function v in E_c converges pointwise to 1 on $\tilde{\Omega}\backslash S_u$ and to 0 on S_u.

The same Γ-convergence results holds for the discrete functional $E_{c,h}$, defined by the projection of E_c over a piecewise affine finite element space, provided that the characteristic length of the mesh, h (defined as the radius of a circle included in or

containing an element) tends to zero faster than the infinitesimals k_c and c (Bellettini and Coscia, 1994). In the following subsection, we discuss the numerical solving of the discrete minimization problem.

2.1.1. Numerical solving of the discrete problem

We propose to minimize the regularized functional for small c's. Note however, that the Γ-convergence result does not provide an error estimate between the minimizers for E and those for $E_{c,h}$, so that we cannot evaluate how close the computed solution is to that of the original problem.

At this stage, quite a few technical issues are to be addressed. Firstly, in view of the presence of the term $v^2|\nabla u|^2$, the functional $E_{c,h}$ is not convex in (u, v). Then, even if the existence of a minimizer is proved, it may not be unique (note that since this is also true of the strong and weak functionals, a regularized functional, the minimizer of which is unique would be a bad candidate for actual numerical use). Further, the convergence criterion is rather ambiguous, and does not guide our choice of the parameters c, k_c, h and of the size of $\tilde{\Omega}$. Let us first describe the minimization of the discrete functional, assuming that the fixed parameters c, k_c and h are already suitable for a good approximation.

Although $E_{c,h}$ is not convex in general, it is convex and coercive in each variable, so that, once one of the fields is fixed, the minimization with respect to the other variable is easy. The idea is then to iterate minimizations in each variable until the successive minimizers are close enough to one another. This alternate minimization method is similar to the relaxation algorithm for quadratic problems (in order to prevent any confusion between the relaxation method for solving quadratic problems and the functional theory of relaxation, we will keep calling the method alternate minimization). Again, we are unable to prove the convergence of this algorithm; the sequence of optimal energies does converge and, up to a subsequence, the alternate minimizers converge to some critical point of $E_{c,h}$. Both minimization problems are implemented by a standard finite element method, with triangular first-order Lagrange elements. As discussed in the next section, it is not required nor desirable to use higher order elements. We remark that the u-problem can be solved in the physical domain Ω, while the v-problem needs to be implemented on the logical domain $\tilde{\Omega}$. Note that, for the sake of simplicity, we use the same triangulation for both problems. The minimization algorithm is then

- *Initialization*

  Fix the regularization parameter c, the mesh size h and the parameter k_c, build a triangulation of $\tilde{\Omega}$ and choose a 'good' starting point v_0.
- *Iteration k*
  1. Compute u_k, minimizing $E_{c,h}(\cdot, v_{k-1})$ on Ω for the given boundary conditions.
  2. Extend u_k by U on $\tilde{\Omega}\backslash\Omega$.
  3. Compute v_k, minimizing $E_{c,h}(u_k, \cdot)$ on $\tilde{\Omega}$.
  4. If $\|v_k - v_{k-1}\|_\infty \geq \epsilon$, perform an additional step; if not, exit.

- *Conclusion*

  Compute the optimal energies, save data and return to the initialization step for the next time step.

The implementation of the next load steps in the study of a monotonically increasing load follows easily. Since it suffices to add an irreversibility criterion on the crack set (i.e., that the cracks do not experience self-healing as the load increases), one should disconnect the nodes where a crack is detected, or, equivalently, add restrictions on the admissible set for the crack field by imposing some homogeneous Dirichlet conditions on the detected crack field v. The second solution is that which has been implemented.

2.1.2. Parameter adjustment

We now discuss the choice of parameters for an actual and efficient numerical implementation of the algorithm. The numerical parameters that have to be set prior to any computation are the logical domain $\tilde{\Omega}$, the regularization parameters c and k_c and the mesh step h. The role of the parameter k_c is easy to understand. It is used to ensure the existence of the minimizers for E_c at fixed c. As far as the solving of the discrete problem is concerned, it is used to prevent the problem from being ill-posed. Assume that $k_c=0$; then, if the v field is numerically equal to zero for a node and for each of its neighbors, the corresponding line of the finite element matrix and of its right-hand-side are both identically equal to zero and the solving of the linear system associated with the finite element problem will diverge. On the contrary, if k_c is too big, then some rigidity will remain in the cracked region, and the bulk energy will be overestimated while the energy restitution of a crack will be underestimated. The choice of this parameter is then a compromise between numerical stability and efficiency.

The choice of the other parameters is more subtle and requires the study of various estimates for the upper and lower Γ-limits. For the sake of simplicity, we only investigate the sequence built for the estimate from above in the Γ-limit in a one-dimensional case. Assume that the crack is at the section $\tau=0$ of the domain, τ being a parameterization of the bar. In that case, the function v, built in the upper Γ-limit estimate is equal to 0 for $|\tau| \leq Ch$, and to $1-\exp(-|\tau|/2c)$ otherwise. Thus, for fixed h and c, the first term is of the order of h/c, which illustrates the hypothesis $h \ll c$. Note that this estimate is independent of the order of the finite element method, so that increasing the accuracy of the discrete approximation through the use of a higher-order interpolation operator will not be beneficial. Note also that this criterion is only required 'close' to the cracks, so fine meshing is only necessary across the cracks.

The estimate for v 'far' from the cracks is useful for understanding how big $\tilde{\Omega}$ should be compared to Ω. Let us neglect the discretization error. The approximation of v far from the jumps of the displacement field implies that the computed surface energy in that region is less than $1/c\int_0^T \exp(-t/c)\mathrm{d}t$, where $T=\mathrm{dist}(S_u,\ \partial\tilde{\Omega})$. So the error on the surface energy term is of the order of $\exp(-T/c)$.

The last parameter is the regularization constant, c. Its influence on the computed energy and minimizers has a mechanical interpretation: E_c resembles a damage model where v is the damage variable. This is however, a mere mathematical artifact, although it does establish the convergence of a very specific damage model to a fracture model. In this context, the parameter c can be interpreted as a characteristic damage scale; a softening phenomenon takes place across the crack, causing the bulk energy to be underestimated.

The previous considerations can be summarized as follows:

- c must be chosen small enough to prevent a softening effect that causes the bulk energy to be underestimated and large enough compared to the discretization step h near the cracks, so as not to overestimate the surface energy.
- k_c must be big enough to prevent the numerical scheme from diverging but small enough, so as not to overestimate the bulk energy near the crack.
- The logical domain must be tailored to c, so as to adequately estimate the energy of cracks near the boundary of the physical domain.

Our remarks on the shape of the approximating crack field permit an easy implementation of an adaptive mesh strategy where the v field is used as an error estimator in a mesh generator that refines the triangulation wherever h is close to 0 (close to the cracks), and possibly enlarges elements elsewhere. This kind of adaptive approach seems very promising in terms of computational cost. Indeed, the proposed algorithm forces the solving of an elasticity-like problem (the u-problem) at each alternate minimization step (we have observed up to 150 such steps for a single loading step). Thus, any improvement in the finite element process (assembly, linear system solving) could drastically reduce the computational cost.

The last datum to be set before starting the algorithm is the starting point v_0. For want of uniqueness of the minimizers, the algorithm will be sensitive to the choice of v_0. As first time step in a discrete time scheme, we choose $v_0 \equiv 1$. At the next time step, we can choose either to reuse the last computed field v or to start again with $v_0 \equiv 1$. In the numerical experiments presented below, we initialize $v_0 \equiv 1$ at each time step.

2.2. Approximation by means of adaptive finite elements

In this section, we briefly detail the implementation of a second approximation that makes an extensive use of the mesh adaptation techniques. The method is based on that developed for the Mumford–Shah problem in Bourdin and Chambolle (1999), where the numerical implementation and the mathematical properties of a variant of an approximation proposed in Chambolle and Dal Maso (1998) is detailed.

The main difference between this method and the previous one is that we try to build a regularized functional defined on a finite element space—a finite dimensional space—instead of discretizing a continuous approximation of E.

Firstly, we define a set of triangulation $\mathscr{T}_h(\tilde{\Omega})$, for each $k \geq 6$ and $0 < \theta_0 \leq 60^\circ$ of $\tilde{\Omega}$, the triangles T of which exhibit the following characteristics:

- The length of all three edges of T lies between h and kh.
- The three angles of T are greater than or equal to θ_0.

We call $V_c(\tilde{\Omega})$, the set of continuous and piecewise affine functions of $\tilde{\Omega}$ and, for $u \in V_c(\tilde{\Omega})$, $\mathscr{T}_h(u) \subseteq \mathscr{T}_h(\tilde{\Omega})$, the set of all triangulations adapted to u, i.e., such that u belongs to the Lagrange first-order finite element induced by $\mathscr{T}_h(\tilde{\Omega})$. Then, we consider a non-decreasing concave function f: $[0, +\infty) \to [0, +\infty)$ such that

$$\lim_{t \downarrow 0} \frac{f(t)}{t} = 1 \quad \text{and} \quad \lim_{t \to +\infty} f(t) = 1/3,$$

for example $f(t) = 2 \tan^{-1}(3\pi t/2)/3\pi$. For each piecewise constant function v, defined on a triangulation $\mathbf{T}$, we denote by v_T its value on the element $T \in \mathbf{T}$ and define the following regularizing operators

$$(Mv)_T = M_T(v) = \frac{\displaystyle\sum_{T' \in \mathbf{T},\ T' \cap T \neq \varnothing} | T' \cap \tilde{\Omega} |\, v_{T'}}{\displaystyle\sum_{T' \in \mathbf{T},\ T' \cap T \neq \varnothing} | T' \cap \tilde{\Omega} |} \tag{4}$$

and its adjoint

$$(M^* v)_T = M_T^*(v) = \sum_{T' \in \mathbf{T},\ T' \cap T \neq \varnothing} \frac{| T' \cap \tilde{\Omega} |}{S_{T'}} v_{T'}, \tag{5}$$

where $S_T = \Sigma_{T' \cap T \neq \varnothing} | T' \cap \tilde{\Omega} |$. Then, for each $u \in L^2(\tilde{\Omega})$ and each $\mathbf{T} \in \mathscr{T}_h(\tilde{\Omega})$, we define the functional

$$G_h(u, \mathbf{T}) = \begin{cases} \displaystyle\sum_{T \in \mathbf{T}} | T \cap \tilde{\Omega} | \, \frac{1}{h_T} f(h_t M_T^*(| \nabla u |^2)), & \text{if } u \in V_h(\tilde{\Omega}),\ \mathbf{T} \in \mathscr{T}(u), \\ +\infty, & \text{otherwise,} \end{cases} \tag{6}$$

and

$$G_h(u) = \min_{\mathbf{T} \in \mathscr{T}_h(\tilde{\Omega})} G_h(u, \mathbf{T}). \tag{7}$$

It is proved in Bourdin and Chambolle (1999) that there exists $\Theta > 0$ such that if $\theta_0 \geq \Theta$ then as $h \to 0$, G_h $\Gamma(L^2(\tilde{\Omega}))$-converges to the functional defined on L^2 by

$$G(u) = \begin{cases} \int_{\tilde{\Omega}} |\nabla u|^2 \, \mathrm{d}x + \mathscr{H}^1(S_u), & \text{if } u \in L^2(\tilde{\Omega}) \cap \mathrm{GSBV}(\tilde{\Omega}), \\ +\infty, & \text{if } u \in L^2(\tilde{\Omega}) \backslash \mathrm{GSBV}(\tilde{\Omega}), \end{cases} \tag{8}$$

where $\mathrm{GSBV}(\tilde{\Omega})$ is the space of functions such that all their truncates lie in $\mathrm{SBV}(\tilde{\Omega})$.

According to the remarks made in the previous sections, we now wish to minimize G_h for a small h. Recall that the mesh itself is a minimization variable; the construction for the estimate from above in the Γ-limit shows how to build the optimal triangulation, given the optimal displacement field u, for the approximated functional (7). This minimizer u being obviously unknown (since it is exactly what we are trying to compute), we propose to deduce some nearly optimal triangulation from a previously computed approximation u_ϵ, assuming that it is 'close' to u. The following iterative algorithm that can also be seen as a relaxation algorithm between the two unknowns is proposed for the solving of (6):

- *Initialization* (background mesh generation):
  Given h_0, choose an arbitrary (regular) triangulation $\mathbf{T}_{h_0}$.
- *Iteration i* (minimization process):
  1. Find u_i solving $\min_{u \in V_{h_i}(\tilde{\Omega})} G_{h_i}(u, \mathbf{T}_{h_i})$ with prescribed value U on $\tilde{\Omega} \backslash \bar{\Omega}$.
  2. Mesh adaptation: build the mesh $\mathbf{T}_{h_{i+1}}$ for u_i and h_{i+1} (possibly equal to h_i).

Note that we do not know how to truly minimize (6) with respect to the triangulation, and merely estimate a near optimal triangulation, used in the construction of the upper Γ-limit.

The minimization with respect to u is addressed through a dualization technique where an auxiliary variable v, constant on each element, is introduced; it relies on elementary properties of the Fenchel transform. Assume that f is differentiable and extend it by $-\infty$ on $]-\infty, 0]$. The Fenchel transform of $-f$ is

$$\psi(-v) = \sup_{t \in \mathbf{R}} \{tv - (-f)(t)\} = (-f)^*(v).$$

By a classical result (see for example Ekeland and Temam, 1976), $(-f)^{**} = -f$, so that

$$-f(t) = \sup_{v \in \mathbf{R}} \{tv - \psi(-v)\} = \inf_{v \in \mathbf{R}} \{tv + \psi(v)\}.$$

Hence,

$$f(t) = \min_{v \in [0,\ 1]} \{tv + \psi(v)\}$$

and the minimum is reached for $v = f'(t)$, so that $v(t)$ varies between 0 and 1. Given $\mathbf{T}_h$, the minimization of (6) is then equivalent to that of

$$\sum_{T\in\mathbf{T}_h} | T\cap\Omega | \left(v_T M_T^*(| \nabla u |^2) + \frac{\psi(v_T)}{h_T} \right) \tag{9}$$

which is again implemented by an alternative minimization scheme between both variable u and v. While the u-problem is solved by a finite element method, given u and the triangulation, the optimal value for $M_T(v)$ is given by

$$M_T(v) = M_T(f'(hM^*(| \nabla u |^2));$$

thus, we do not explicitly compute ψ or v.

The boundary conditions on u are taken into account in a way similar to that of the previous method: the 'physical' domain is extended into a 'logical' domain, where the displacement field is fixed at its boundary value U, and the boundary of the 'physical' domain is cracked (its nodes are disconnected) along its Neumann part $\mathcal{N}$.

It is easily seen that if u wants to jump across a triangle T then $M_T^*(|\nabla u|^2)$ tends to $+\infty$ with h and thus, v_T tends to 0 with h, while otherwise $M_T^*(|\nabla u|^2)$ tends to 1 thus, v_T as well, hence, v_T plays in the present context, a role similar to that of the v-field in the first approximation method. The irreversibility of the crack field for an increasing load is addressed by forcing the v_T-field for the time step i to remain equal to zero if it is so at the time $i-1$.

The description of the triangulation adapted to u is the following: 'close' to the jump set of u, the triangles are as flat as feasible within the admissible class and thus 'follow' the crack field, while, 'far' from the jump, there is no recipe on how to position the elements. Therefore, we use an anisotropic mesh generator, and build an estimator defined at each node of the triangulation by a metric, itself built from the value of the v-field and the gradient of the displacement field u. For a detailed discussion on anisotropic mesh adaptation, refer to Borouchaki and Laug (1996).

2.3. Mutual advantages of both methods

Since we cannot prove convergence, a comparison between results computed by the two different methods can help to decide on the reliability of the numerical simulations. We illustrate with an example that the results of both methods seem satisfactory and refer the reader to Subsection 3.1 where the tearing of a reinforcement provides a benchmark for that comparison.

In the light of Subsection 3.1 below the following is not without merit: the first method seems very stable and will, for a sound choice of parameters c, k_c and h, give a good estimate of the different terms of the energy $\mathscr{E}$. On the other hand, the second method is very fast, because the solution of the v-problem is explicitly given, and also because after each adaptation step the number of nodes of the adapted mesh can be reduced [in the example of Fig. 2, the first mesh (2(a)) is made of 2615 nodes while the last one (2(c)) is made of only 1005].

2.4. Remarks on the plane elasticity case

The study of the plane elasticity problem is still in its infancy. The equivalence between strong and weak formulation is not established at this time. Furthermore, non-interpenetration of the crack lips should be imposed. The numerical adaptation of the algorithm to a linear isotropic elasticity problem in the absence of unilateral conditions is similar to that of the antiplane case. The regularized functional that has to be minimized is

$$\int_{\Omega\setminus\mathcal{N}} (v^2 + k_c) W(e(u)) \mathrm{d}x + \int_{\tilde{\Omega}\setminus\mathcal{N}} \left(c \mid \nabla v \mid^2 + \frac{(1-v)^2}{4c} \right) \mathrm{d}x, \tag{10}$$

where $W(\xi) = \frac{1}{2}\{\mathrm{tr}(\xi)^2 + 2e(\xi)\cdot e(\xi)\}$ (recall that we have chosen to set all constants at 1). This is the method that has been used for the computations shown in Figs. 3 and 4. The results are satisfactory, but can sometimes give results that are not physically admissible [see for example Fig. 4(f)]. Implementing unilateral conditions is, however, an open problem as of yet for want of the proper regularized functional in place of (10).

3. Numerical experiments

In this section three numerical experiments are described and compared with theoretical predictions, when available. Let us emphasize once again that we do not try and compare our results with those of true experiments—this will be the object of a forthcoming collaborative investigation with experimentalists—but rather strive to test the validity of the presented computations against the theoretical background developed in Francfort and Marigo (1998). The grey level figures presented below represent the v-field for both methods. The crack site is included within the set of points where that field is near zero (shown in dark grey in the figures).

3.1. Tearing of a reinforcement

The tearing of a three-dimensional cylinder of length L can be solved in a closed form as demonstrated in Francfort and Marigo (1998). A cylinder with an annular cross section of respective inner and outer radii 1 and 3 is considered [see Fig. 1(a)]. It is glued on its inner surface to a rigid shaft which is submitted to an increasing coaxial displacement field δ while its outer surface is clamped. Furthermore, the in-section components of the displacement field, as well as the normal component of the normal stress, are zero at both ends ($u_1 = u_2 = \sigma_{33} = 0$, $x_3 = 0,\ L$). The analytical result predicts—within our formulation—the existence of a critical displacement $\delta_c = \sqrt{2\ \log\ 3} \sim 1.48$ such that if δ is less than δ_c, then no cracks will appear and the solution is that of the elastic problem, while if $\delta \geq \delta_c$, a crack will appear over the entire inner boundary of the material with a

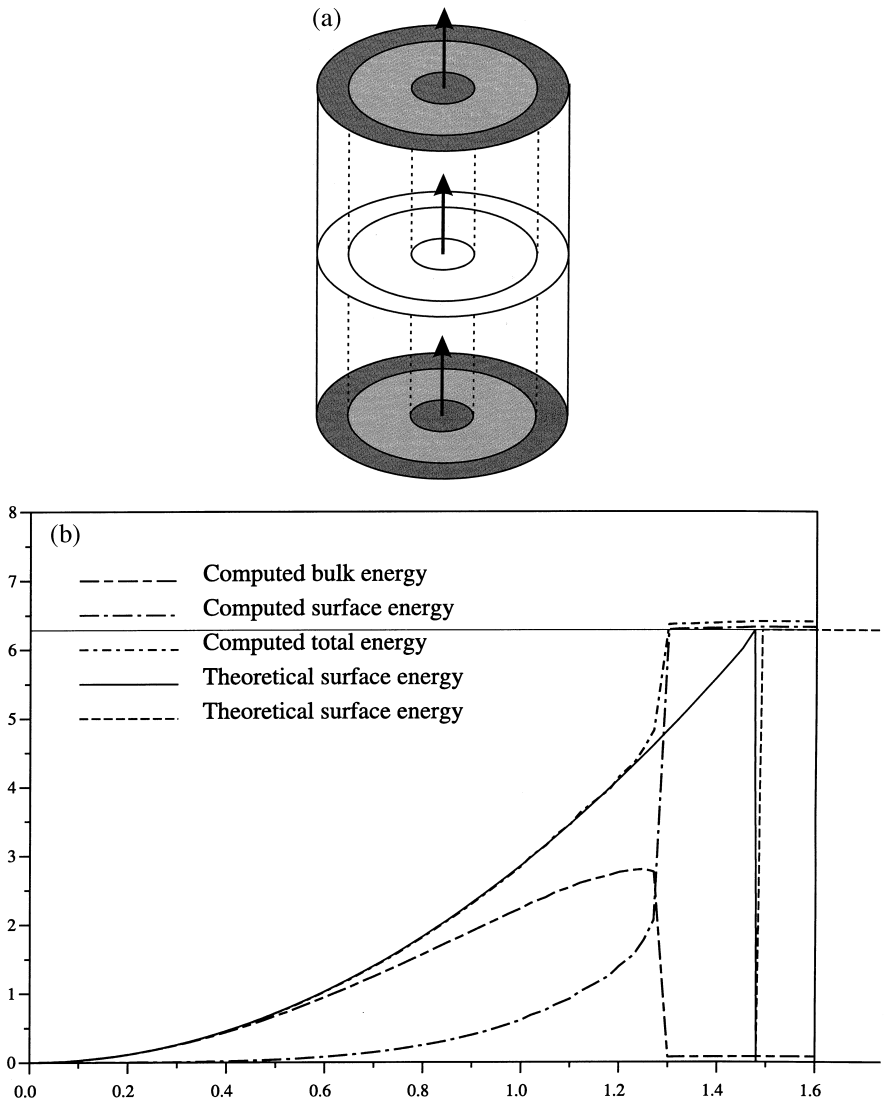

Fig. 1. Tearing of a reinforcement, first method. (a) Geometry and loading. (b) Energy plot (x-axis is the load factor). (c) Mesh. (d) Crack field after failure.

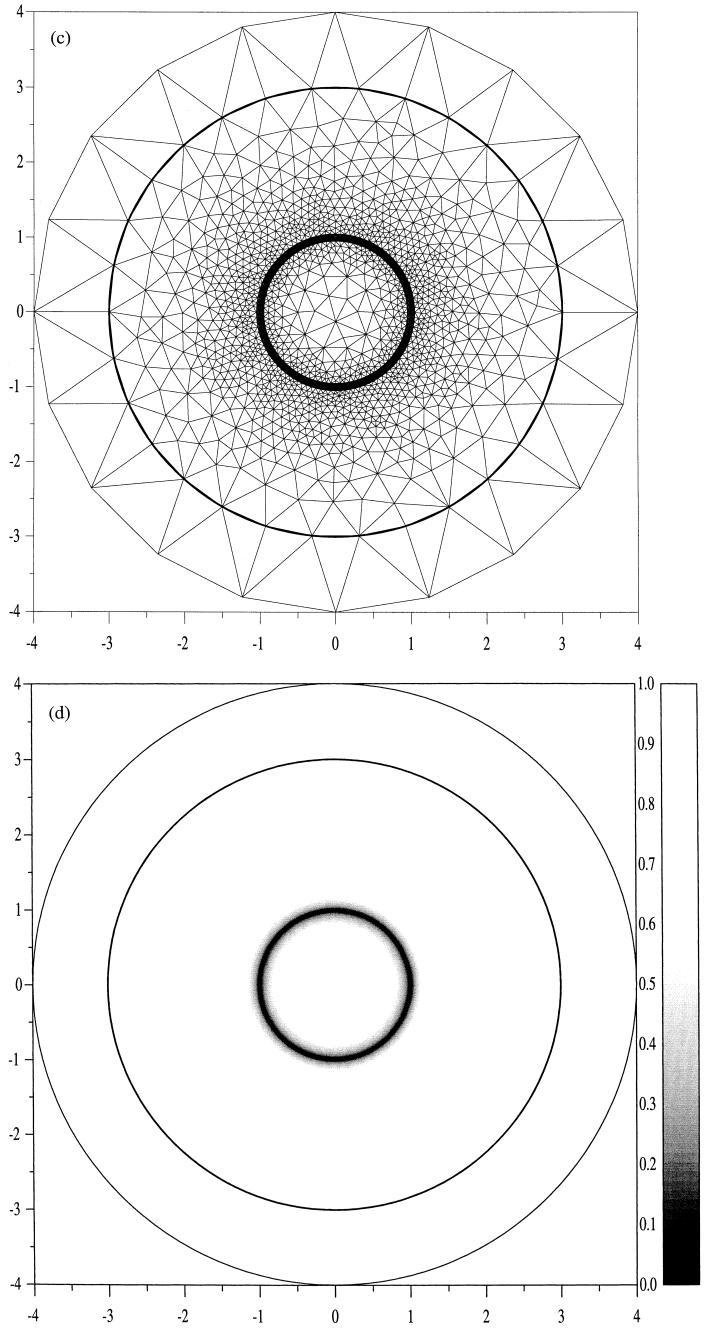

Fig. 1 (*continued*)

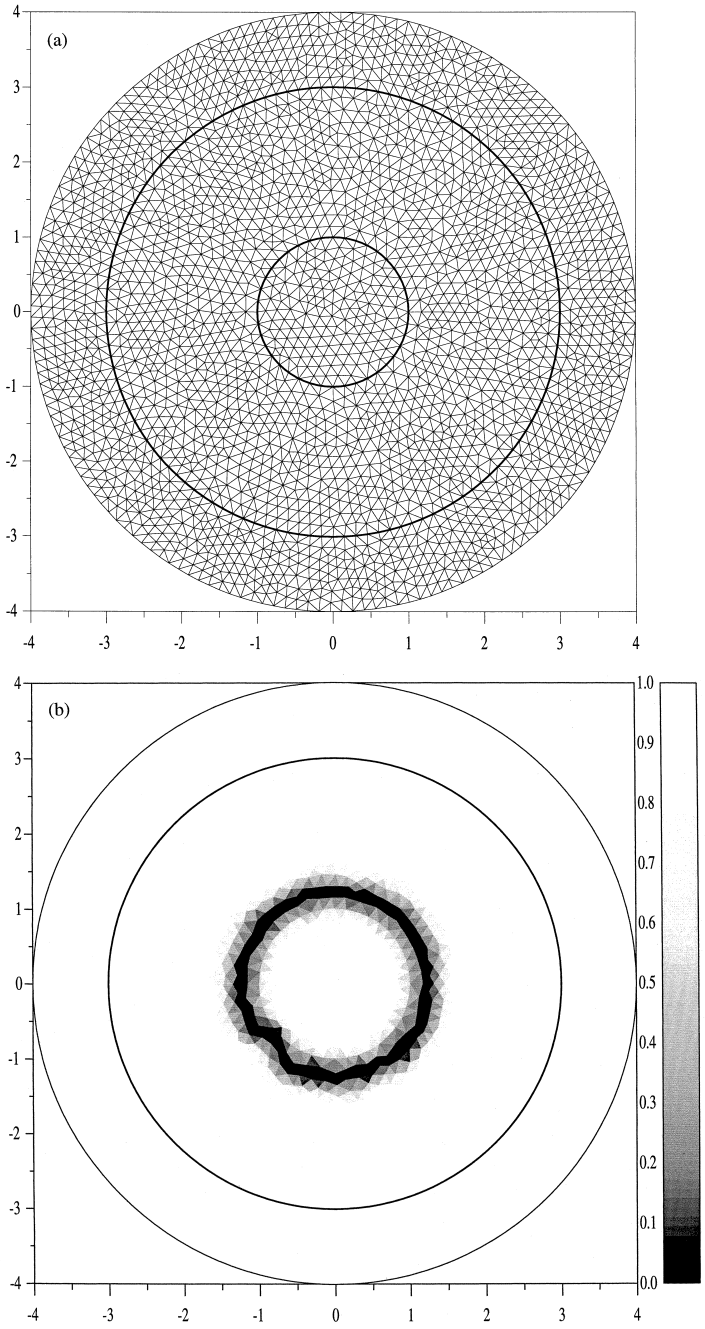

Fig. 2. Tearing of a reinforcement, second method. (a) Background mesh. (b) Crack field for the background mesh. (c) Final mesh. (d) Crack field for the final mesh.

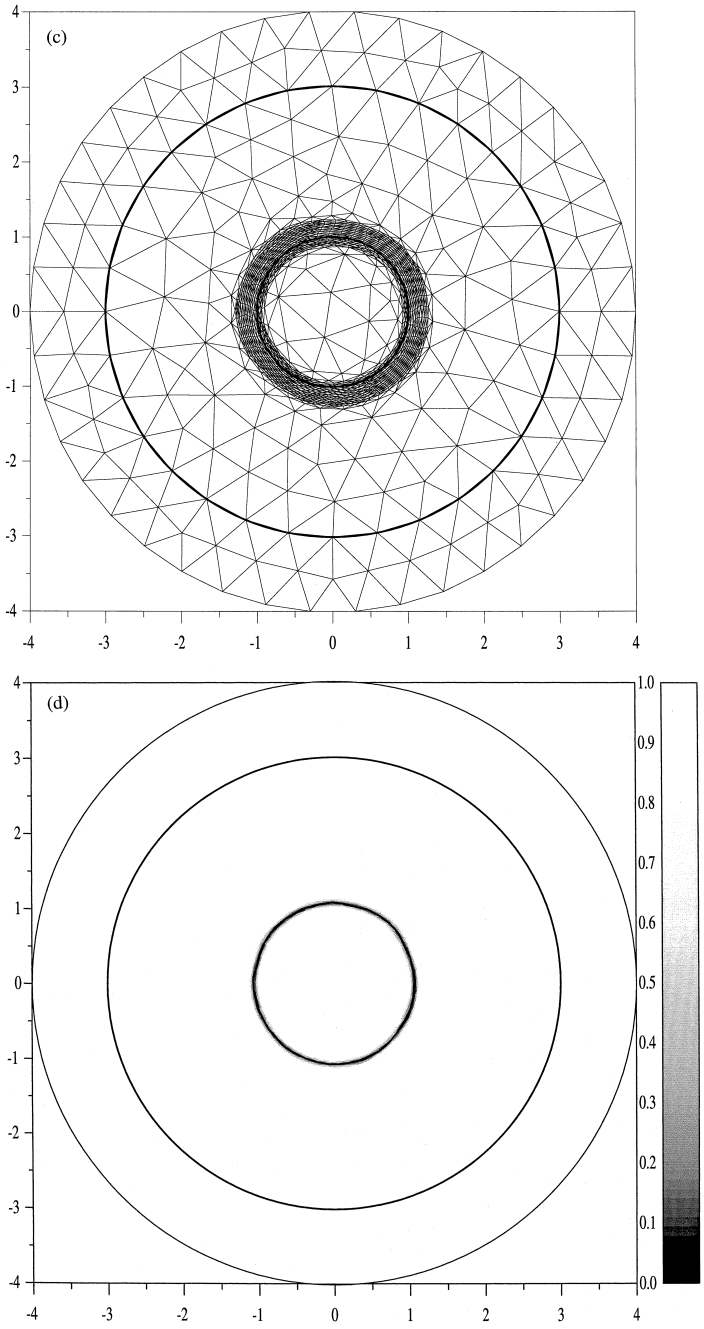

Fig. 2 (*continued*)

surface energy equal to 2π. The computations presented in Fig. 1 are obtained with the first method. The parameters are $h = 10^{-3}$, $c = 10^{-1}$, $k_c = 10^{-4}$. In Fig. 1(b), we plot the bulk energy, surface energy and total energy versus the load δ. The computed critical load is underestimated but the surface energy is correct within 1%. The plot of the crack field [Fig. 1(d)] corresponds to $\delta = 1.5$. In Fig. 2, the same simulation is run with the second method. Figs. 2(a) and (b) represent the first mesh and the corresponding crack field v_T, while in Figs. 2(c) and (d) the mesh has been adapted three times.

Further, both methods yield a continuous dependence of the total energy upon δ (although that dependence is not shown in Fig. 2 in the case of the second method), which is in agreement with the theoretical predictions. Indeed, it is shown in Proposition 4.10 of Francfort and Marigo (1998) that the jump of the elastic energy during brutal crack growth is exactly offset by that of the surface energy; hence, at the time of the total brutal debonding, the total energy should become constant—and equal to 2π—which is exactly the case here.

3.2. Traction experiment on a fiber reinforced matrix

A square elastic matrix is reinforced by a rigid circular fiber as shown in 3(a). The fiber remains fixed while a uniform displacement field δ is imposed on the upper side of the square; the remaining sides are traction-free. The following evolution is observed as δ grows:

1. As long as $\delta < 0.2$, the matrix remains purely elastic. Note however, the presence of spurious surface energy; we are not, after all, computing the Γ-limit but only an approximation, so that the v-field cannot be expected to be identically 1.
2. At $\delta \sim 0.2$, a crack of finite length brutally appears near the north pole of the inclusion [Fig. 3(c)]. This is in agreement with item 4 of Proposition 4.19 in Francfort and Marigo (1998) (brutal crack growth at finite initiation time in the absence of singular points for the purely elastic solution).
3. When δ varies between 0.2 and 0.32, the crack progressively grows in the matrix [Fig. 3(d)].
4. At $\delta \sim 0.32$, the right-hand-side of the matrix is brutally cut [Fig. 3(e)]. Once again this feature agrees with the theoretical predictions of Remark 4.21 in Francfort and Marigo (1998).
5. When δ varies between 0.32 and 0.37, the left part of the crack progressively grows [Fig. 3(f)].
6. At $\delta \sim 0.37$, the crack brutally severs the remaining filament of uncracked material [Fig. 3(g)]. Remark 4.21 in Francfort and Marigo (1998) equally applies here.
7. The sample is split into two parts. Note however, some spurious elastic energy in Fig. 3(g) caused by the coefficient k_c in the functional.

As in the previous computations of Subsection 3.1, there is (nearly) no

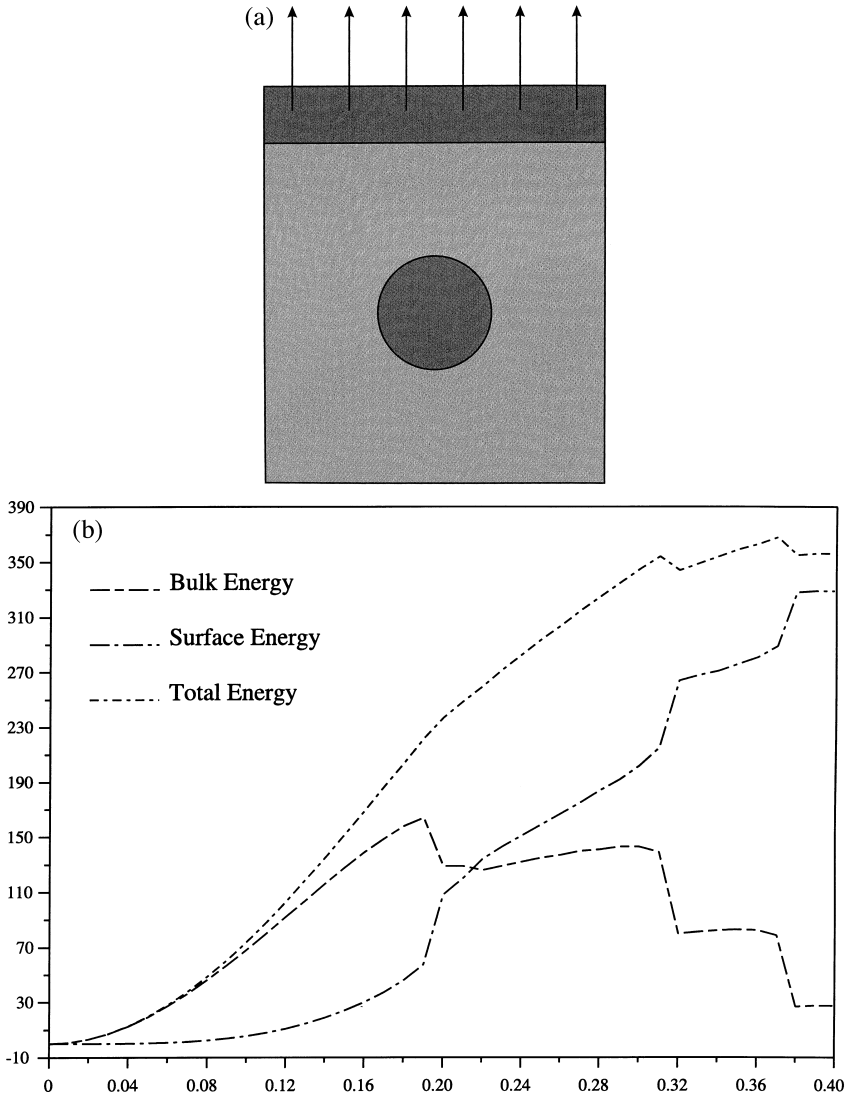

Fig. 3. Traction experiment on a fiber reinforced matrix. (a) Geometry and loading. (b) Energy plot (x-axis is the load factor). (c) Crack field, load is 0.2. (d) Crack field, load is 0.31. (e) Crack field, load is 0.32. (f) Crack field, load is 0.36. (g) Crack field, load is 0.37. (h) Check of Griffith criterion.

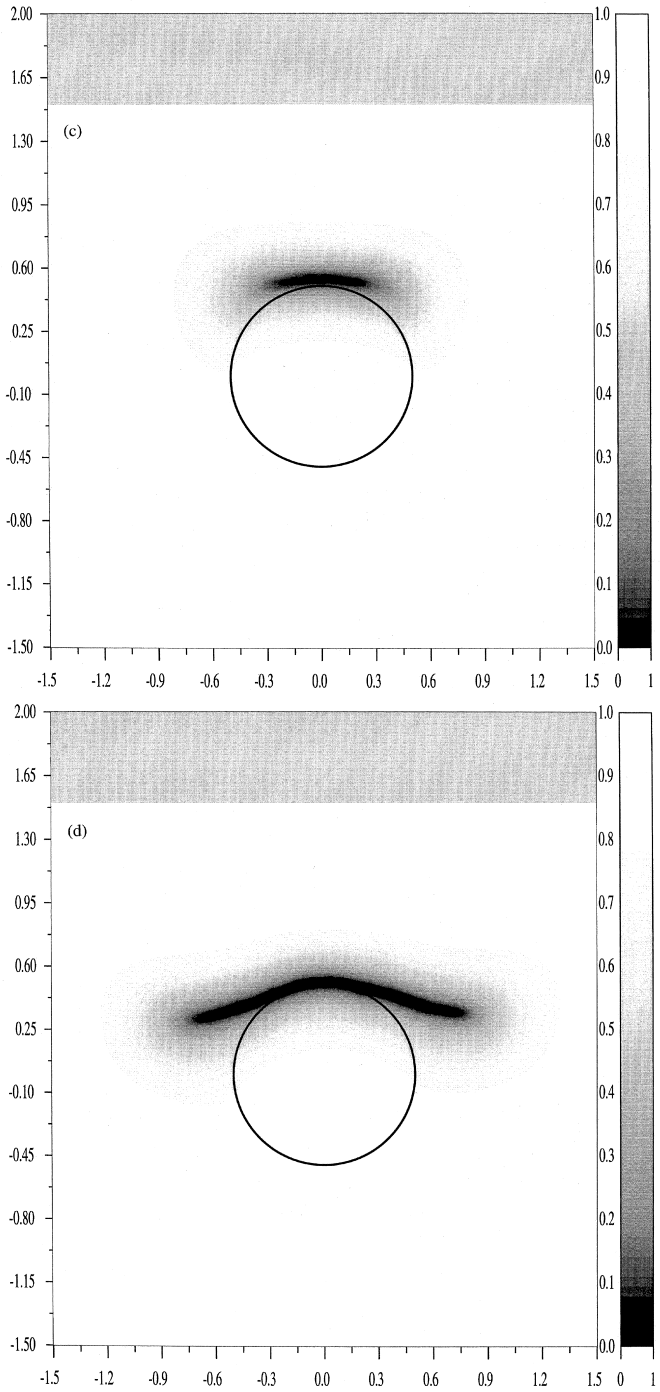

Fig. 3 (*continued*)

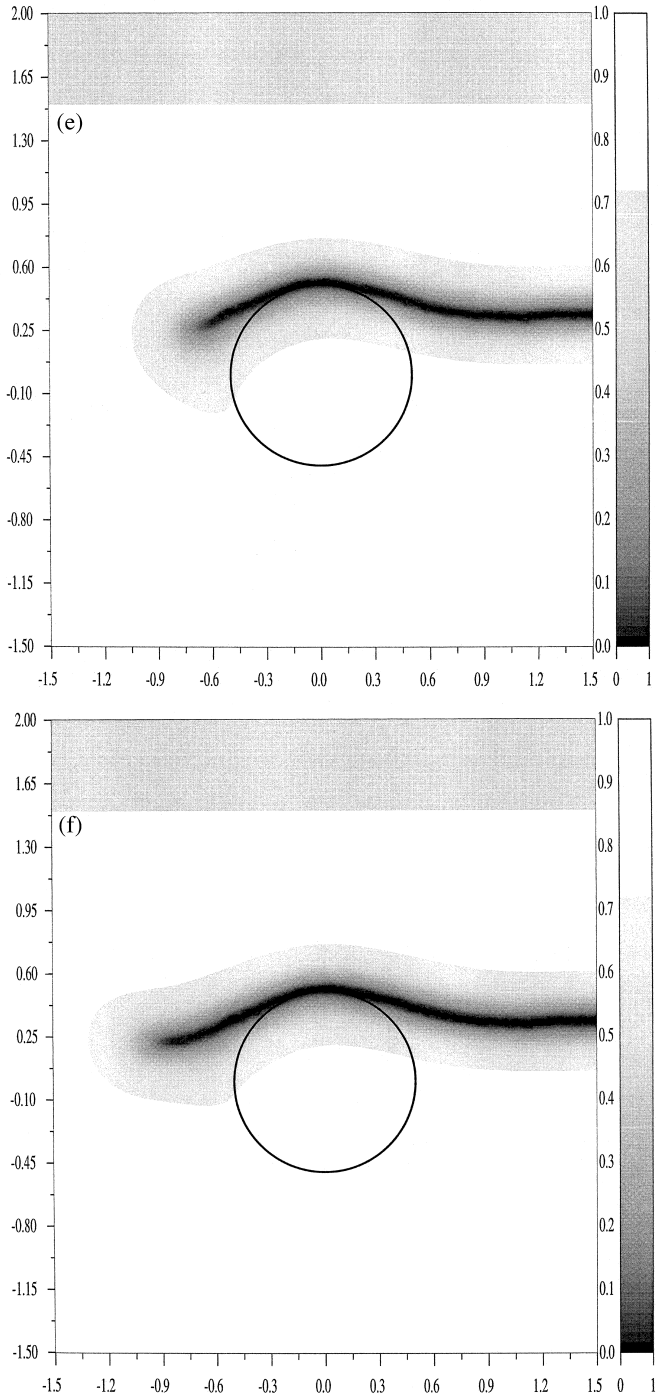

Fig. 3 (*continued*)

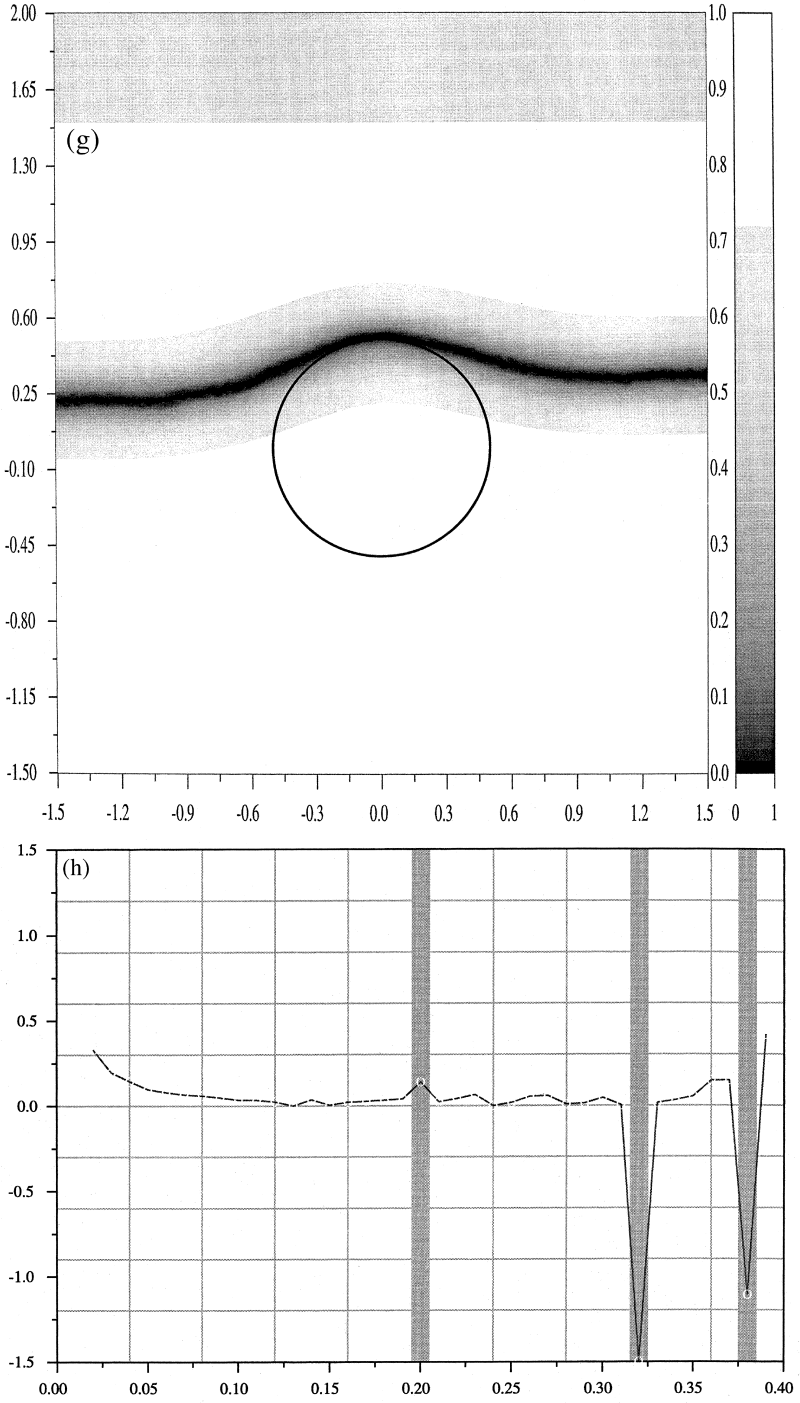

Fig. 3 (*continued*)

discontinuity in the total energy during the phases 2, 4 and 6 of brutal growth, as theoretically expected.

Fig. 3(h) is an attempt at checking the validity of the classical Griffith criterion during crack growth; elementary considerations yield the following criterion in our setting:

$$E'(\delta) = \frac{2E_e(\delta)}{\delta}$$

where $E(\delta)$ is the total energy and $E_e(\delta)$ the bulk energy for a given value of δ. As clearly demonstrated in that figure, the criterion is indeed met during the progressive phases of the evolution

Remark. The symmetry breaking evolution for $\delta \geq 0.32$ might seem somewhat disconcerting. We do not have a definite explanation as of yet. The actual minimum could indeed be asymmetric. We could also possibly be unwillingly trapped around a local minimum; a heuristic solution would then consist in a random sampling of initial guesses, a rather costly undertaking.

Note that the symmetry breaking direction is purely numerical; the used mesh has been chosen asymmetric, so as to ascertain the reality of lateral symmetry whenever an output of the computations.

Remark. Initiation and failure loads, respectively, $\delta_i = 0.2$ and $\delta_f = 0.37$ fall within the theoretically predicted range of Proposition 4.6 in Francfort and Marigo (1998), namely

$$\delta_i \leq 0.222 \leq \delta_f,$$

where the value 0.222 has been estimated from the plot [Fig. 3(b)] by noting that the elastic energy is $\sim$230 when $\delta \sim 0.195$ and thus, that it is $\sim$6000 when $\delta = 1$ because it scales like δ^2.

Remark. This numerical experiment is exemplary because of the wide range of associated crack behaviors throughout the evolution: brutal versus progressive, edge and bulk fracture, ... Furthermore, there seems to be good qualitative agreement between our results and the experimental observations found in Hull (1981).

3.3. Crack branching

The branching of a crack is one of the conundrums of brittle fracture. The classical Griffith theory is inadequate and additional criteria have to be introduced

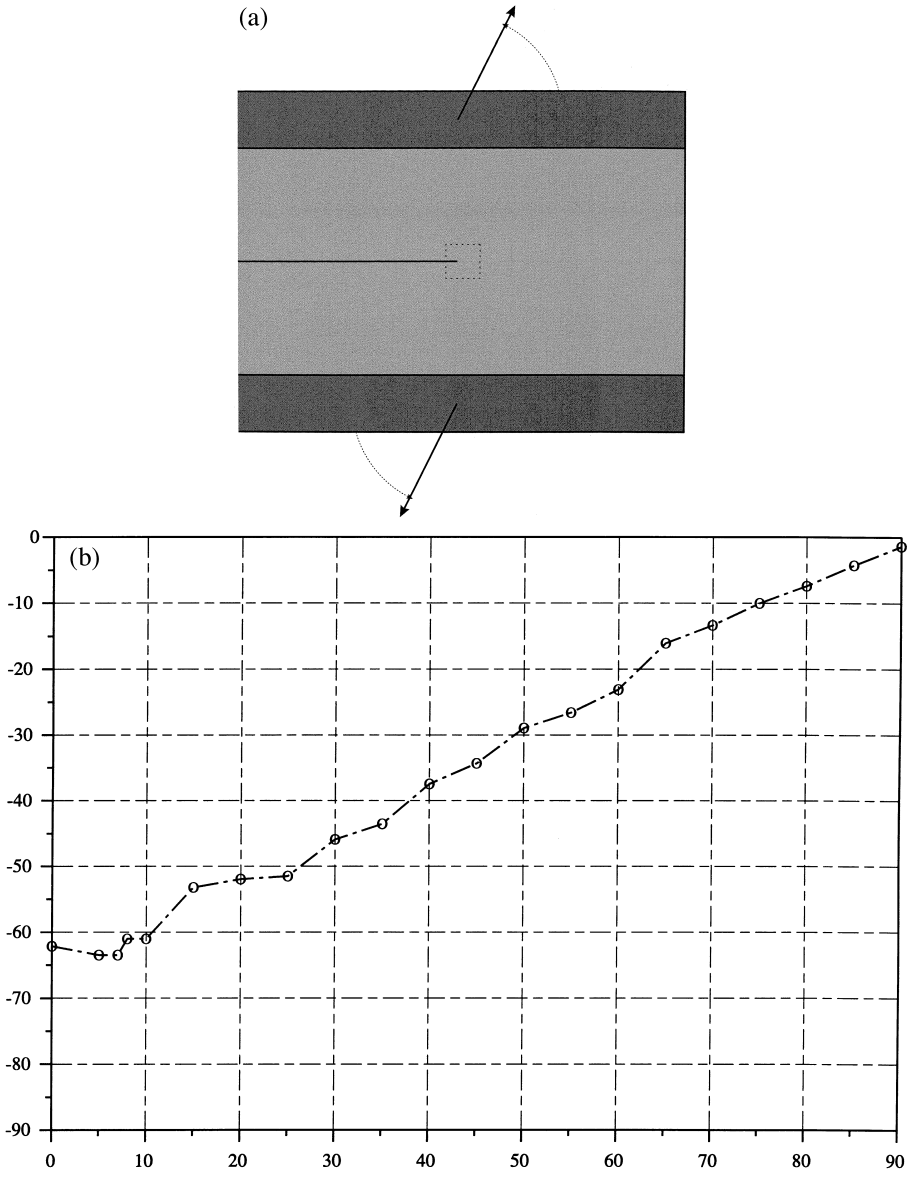

Fig. 4. Branching of a pre-existing crack. (a) Geometry and loading. (b) Computed crack angle (x-axis) vs. load angle (y-axis). (c) Crack field for $\theta = 90°$. (d) Crack field for $\theta = 45°$. (e) Crack field for $\theta = 7°$. (f) Crack field for $\theta = 0°$.

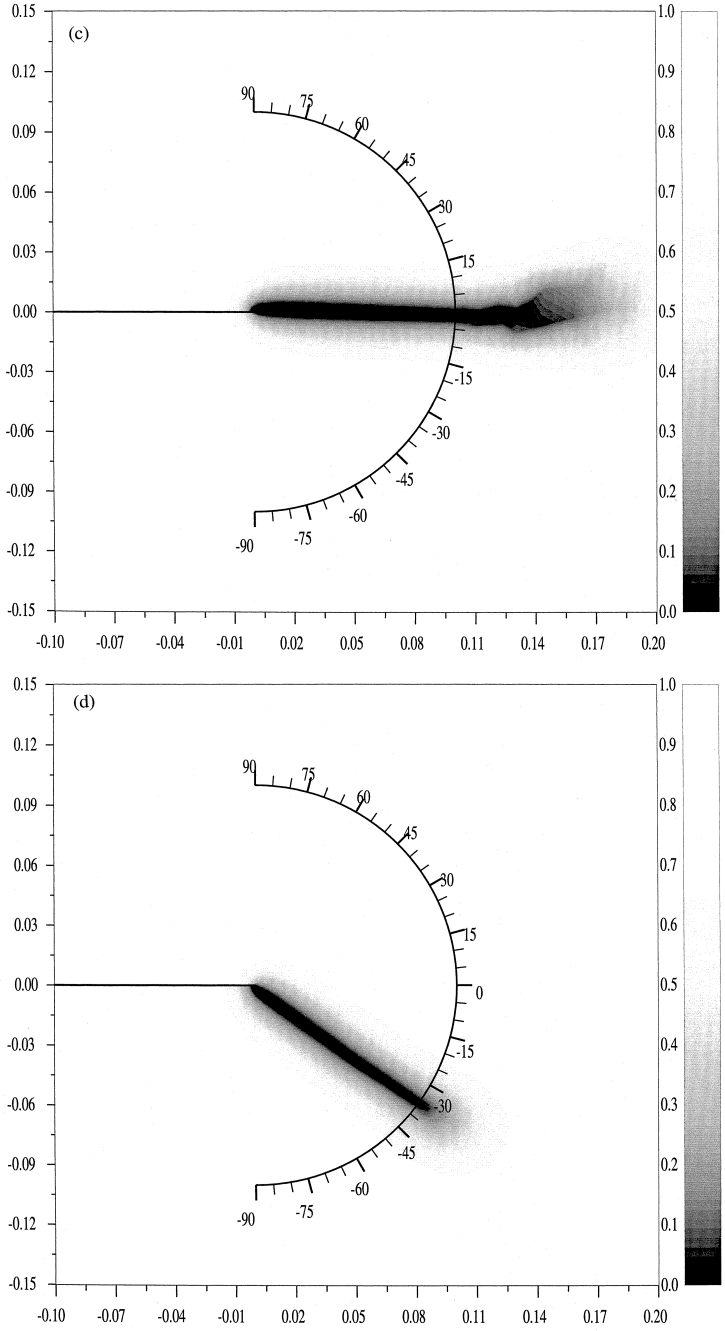

Fig. 4 (*continued*)

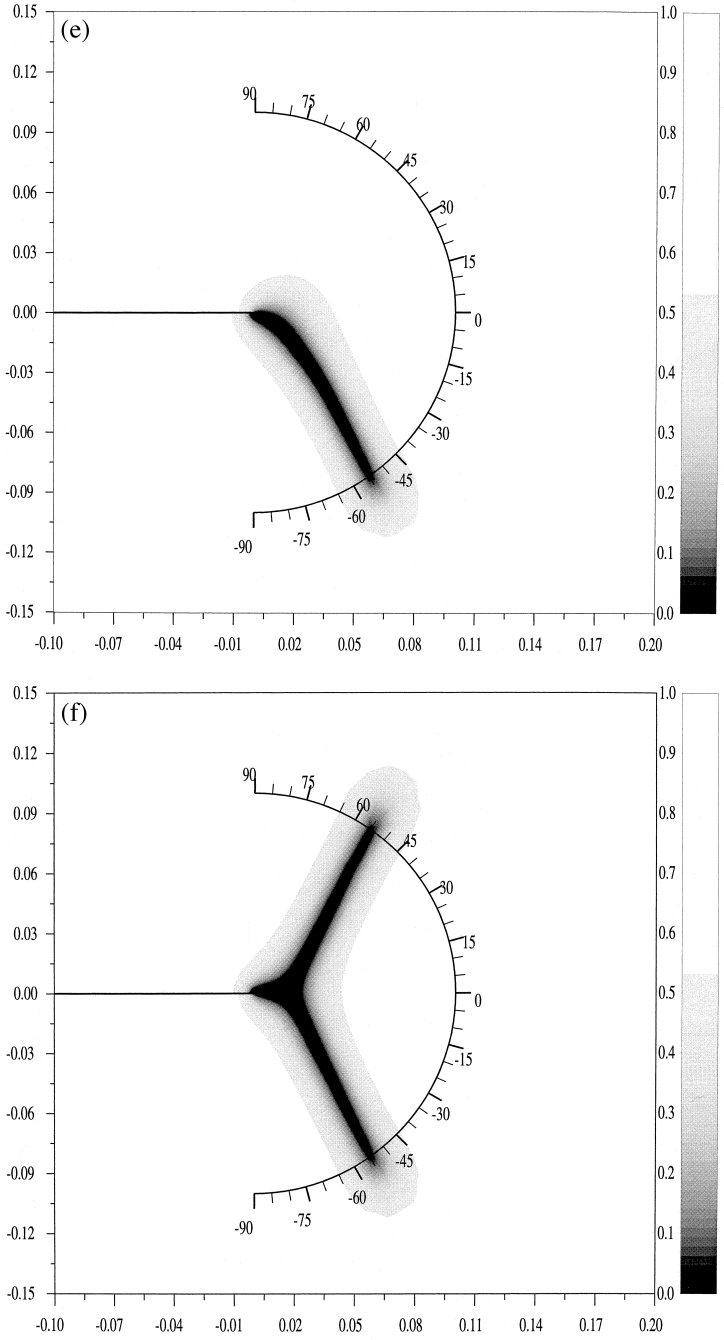

Fig. 4 (*continued*)

(see e.g. Amestoy, 1987; Amestoy and Leblond, 1989; Leblond, 1989; Leguillon, 1993).

In contrast, our formulation permits branching predictions with no added ingredients as will be demonstrated below. A cracked 2-D rectangular elastic sample is investigated. The crack is parallel to the upper and lower sides of the rectangle and a displacement field of increasing intensity δ and fixed orientation θ is applied to those sides [Fig. 4(a)]. The crack evolution is numerically monitored for several values of θ.

1. When $\theta = 90^\circ$, the crack propagates, as expected, along the horizontal axis for a critical value for δ [Fig. 4(c)].
2. When $7^\circ < \theta < 90^\circ$, the crack branches out from the initial crack tip at some θ-dependent angle for a critical value of δ [Figs. 4(d) and (e)].
3. When $0^\circ < \theta < 7^\circ$, the crack develops two symmetric branches for a θ-dependent critical value for δ [Fig. 4(f)]. This result does not conform to existing predictions (see e.g. Amestoy, 1987). It should be noted however, that the upper branch of the crack interpenetrates the sample, which is not allowed in the classical modeling of crack branching. An adequate rendering of the non-interpenetration condition should hopefully rule out the unrealistic upper branching, but this is merely wishful thinking at this time.

References

Ambrosio, L., 1989a. Variational problems in SBV and image segmentation. Acta Appl. Math. 17, 1–40.

Ambrosio, L., 1989b. A compactness theorem for a special class of functions of bounded variation. Boll. Un. Mat. Ital. 3 (B), 857–881.

Ambrosio, L., 1990. Existence theory for a new class of variational problems. Arch. Rational Mech. Anal. 111 (1), 291–322.

Ambrosio, L., Tortorelli, V.M., 1990. Approximation of functional depending on jumps by elliptic functionals via Γ-convergence. Comm. Pure Appl. Math. XLIII, 999–1036.

Ambrosio, L., Tortorelli, V.M., 1992. On the approximation of free discontinuity problems. Boll. Un. Mat. Ital. 7 (6B), 105–123.

Amestoy, M., 1987. Propagations de fissures en élasticité plane. Thèse d'Etat, Paris.

Amestoy, M., Leblond, J-B., 1989. Crack path in plane situation—II, detailed form of the expansion of the stress intensity factors. Int. J. Solids Structures 29 (4), 465–501.

Bellettini, G., Coscia, A., 1994. Discrete approximation of a free discontinuity problem. Numer. Funct. Anal. Optim. 15, 105–123.

Borouchaki, H., Laug, P., 1996. Maillage de courbes gouverné par une carte de métriques. Technical Report RR-2818, INRIA.

Bourdin, B., 1999. Image segmentation with a finite element method. RAIRO Modél. Math. Anal. Numér. 33 (2), 229–244.

Bourdin, B., 1998. Une formulation variationnelle en mécanique de la rupture, théorie et mise en œuvre numérique. Thèse de Doctorat, Université Paris Nord.

Bourdin, B., Chambolle, A., 1999. Implementation of an adaptive finite element approximation of the Mumford–Shah functional (in preparation).

Carriero, M., Leaci, A., 1990. Existence theorem for a Dirichlet problem with free discontinuity set. Nonlinear Anal., Th. Meth. Appls. 15 (7), 661–677.

Chambolle, A., 1998. Finite differences discretizations of the Mumford–Shah functional. RAIRO Modél. Math. Anal. Numér. 33 (2), 261–288.

Chambolle, A., Dal Maso, G., 1998. Discrete approximation of the Mumford–Shah functional in dimension two. RAIRO Modél. Math. Anal. Numér. (in preparation).

De-Giorgi, E., Carriero, M., Leaci, A., 1989. Existence theorem for a minimum problem with free discontinuity set. Arch. Rational Mech. Anal. 108, 195–218.

Ekeland, I., Temam, R., 1976. Convex Analysis and Variational Problems. North-Holland, Amsterdam.

Finzi-Vita, S., Perugia, P., 1995. Some numerical experiments on the variational approach to image segmentation. In: Proceedings of the Second European Workshop on Image Processing and Mean Curvature Motion, Palma de Mallorca, pp. 233–240 (25–27 September).

Francfort, G., Marigo, J-J., 1998. Revisiting brittle fracture as an energy minimization problem. J. Mech. Phys. Solids 46 (8), 1319–1342.

Hull, D., 1981. An Introduction to Composite Materials. Cambridge University Press, Cambridge, Solid State Science Series.

Leblond, J-B., 1989. Crack paths in plane situation—I, general form of the expansion of the stress intensity factors. Int. J. Solids Structures 25, 1311–1325.

Leguillon, D., 1993. Asymptotic and numerical analysis of a crack branching in non-isotropic materials. Eur. J. Mech. A/Solids 12 (1), 33–51.

Modica, L., Mortola, S., 1977. Un esempio di Γ-convergenza. Boll. Un. Mat. Ital. 14B, 285–299.

Mumford, D., Shah, J., 1989. Optimal approximation by piecewise smooth functions and associated variational problems. Comm. Pure Appl. Math. 42, 577–685.